BMC Research Notes

RESEARCH NOTE

Open Access

Investigation the role of *SIRT3*, *SIRT7*, *NFATC1*, and *PDL-1* genes in androgenetic alopecia

Hadis Abbasian[1], Mehrdad Noruzinia[1] and Masoud Garshasbi[1*]

Abstract

Background Androgenetic alopecia (AGA) stands as the most prevalent form of hair loss, affecting the hair follicles (HFs). Aging emerges as a prominent contributor in this condition. In this study, our aim is to elucidate the expression patterns of candidate genes—*SIRT3*, *SIRT7*, *NFATC1*, and *PDL-1*—known to exhibit differential expression levels during HF aging, and to underscore the role of aging in AGA.

Material and methods Mesenchymal stem cells (MSCs) were isolated from the vertex and occipital regions of six men affected by AGA. The aim was to assess the expression levels of *SIRT3*, *SIRT7*, *NFATC1*, and *PDL-1* genes. RNA extraction was performed followed by cDNA synthesis, and gene expression levels were quantified using real-time PCR. To validate the experimental findings, two different RNA-seq datasets relevant to the study were analyzed using R software.

Results In the present study, experimental tests revealed that the expression levels of *SIRT3* and *SIRT7*, known to decrease during HF aging, were diminished in AGA-affected samples as well. Conversely, the mean value of *NFATC1* and *PDL-1* expression level, which are known to increase during HF aging, were found to be elevated in AGA-affected samples. Moreover, bioinformatic analyses provide additional support for the role of *SIRT3*, *SIRT7* and *NFATC1*in AGA pathogenesis.

Conclusion While *SIRT3* and *SIRT7* may play critical roles in AGA development, further research is needed to elucidate the significance of *NFATC1* and *PDL-1* in this context and to explore their potential as therapeutic targets for AGA treatment.

Keywords Androgenetic alopecia, *SIRT7*, *SIRT3*, *NFATC1*, *PDL1*

Introduction

Androgenetic alopecia (AGA), characterized by progressive hair thinning and eventual baldness, represents the most prevalent form of hair loss in humans [1]. While AGA itself does not pose an immediate medical emergency condition, its psychological implications can profoundly impact patients' self-esteem and mental well-being [2]. The common pattern of baldness observed in men, referred to as the Hamilton-Norwood classification [3], is distinguished by a sequential reduction in hair density along the forehead, followed by progressive thinning and eventual loss of hair on the vertex, leaving only the parietal and occipital areas with dense hair coverage. the prevalence of AGA escalates with advancing age, albeit the rate and extent of progression vary significantly among individuals [4].

The pathogenesis of AGA is intricately linked to dysregulation of the hair cycle [5] and the consequent miniaturization of hair follicles (HF) [6, 7]. Notably, the dysregulation primarily affects hair follicle stem cells (HFSCs), contributing significantly to the pathologic manifestations of AGA [8]. During each hair cycle,

*Correspondence:
Masoud Garshasbi
masoud.garshasbi@modares.ac.ir
[1] Department of Medical Genetic, Faculty of Medical Sciences, Tarbiat Modares University, Tehran, Iran

active HFSCs undergo division, giving rise to various cell types within the HF during the Anagen phase [9]. Subsequently, these stem cells enter a quiescent state during the Telogen phase [10]. HFSCs in individuals affected by AGA exhibit an extended Telogen phase compared to their healthy counterparts [5], owing to differential gene expression and altered pathway functions [8]. The dysregulation of stemness is observed in other human pathologies, as well [11, 12].

AGA arises from a complex interplay of genetic predisposition, hormonal influences, environmental factors, and advancing age [13]. In elucidating the role of aging in the context of AGA, the consequential lengthening of the Telogen phase with advancing age, culminates in a reduction in hair density. This phenomenon is attributed to the diminished capacity of HFCs to initiate new hair cycles and produce hair shafts [14]. The insights provided by previous studies offer valuable context for understanding the role of specific genes—*NFATC1*, *SIRT7*, *SIRT3*, and *PDL-1*—in AGA pathogenesis.

NFATC1 has been implicated in maintaining HFSCs in the Telogen phase of the hair cycle, inducing quiescence and inhibiting hair growth [15, 16]. *NFATC1* activity is controlled by some genes such as *SIRT7* [17], and *SIRT7* expression decreases during aging [18]. This interplay suggests a potential link between *NFATC1* dysregulation and aging-related changes in HFSC activity, contributing to AGA progression.

Mitochondrial activity may also be implicated in AGA pathogenesis. *SIRT3*, a mitochondrial deacetylase, exhibits altered expression levels during aging, potentially leading to mitochondrial dysfunction [19]. Considering the vital role of mitochondria in cellular function, dysregulation of *SIRT3* may contribute to AGA progression.

Moreover, the upregulation of *PDL-1* expression during aging, along with its inhibitory role in hair growth observed in mice [20], suggests a potential mechanism by which *PDL-1* dysregulation may contribute to AGA pathogenesis.

In this study, the goal is to validate experimental findings with bioinformatic analyses, thereby enhancing our understanding of the molecular mechanisms underlying AGA.

RNA-Seq technology serves as a pivotal tool for comparing gene expression profiles between different conditions, such as affected tissue in a disease state versus healthy tissue, thereby elucidating the differential regulation of genes in each condition. Among the various computational tools available for analyzing RNA-Seq data, DESeq2 [21] from Bioconductor (http://www.bioconductor.org/) is widely recognized for its effectiveness and reliability [22]. Differential expression (DE) analysis, a cornerstone of RNA-Seq data analysis, facilitates the identification of genes that have different expression [23, 24].

Furthermore, DE analysis enables downstream systems biology analyses, such as gene ontology (GO) analysis, which offers valuable insights into the cellular processes that are altered between different biological conditions [25]. Additionally, DE analysis facilitates the enrichment analysis of biological pathways using resources like the Kyoto Encyclopedia of Genes and Genomes (KEGG) database [26].

Our objective is to evaluate the expression levels of four candidate genes—*NFATC1*, *SIRT3*, *SIRT7*, and *PDL-1*—which exhibit differential expression between aged and youthful cells, between HFSCs affected by AGA and healthy HFSCs.

Material and methods

Mesenchymal stem cells extraction, isolation and expansion

HFs were extracted from the vertex (balding) and occipital (high hair density) regions of six male subjects affected by AGA. The extraction process involved isolating mesenchymal stem cells (MSCs) through mechanical separation techniques. Under microscopic observation, the extracted HFs were meticulously dissected using microdissection tools to isolate the MSCs from the surrounding tissue. Following separation, MSCs were thoroughly washed with phosphate-buffered saline (PBS). Subsequently, the cells were cultured in 25 cm^2 tissue culture flasks, utilizing a medium consisting of 89.5% Dulbecco's Modified Eagle's Medium low glucose (DMEM, Biowest, France), supplemented with 10% fetal bovine serum (FBS, Gibco, USA), and 0.5% Amphotrypsin A antibiotic (Invitrogen, USA), and maintained at 37 °C in an atmosphere of 95% air and 5% CO2. Upon reaching 80 to 90% confluence, the MSCs were trypsinized using 0.25% trypsin EDTA (Biowest, France), followed by media replacement. This methodology ensured the successful isolation and cultivation of HFSCs for subsequent analyses. Finally, to characterize and quantify the expression of MSCs markers based on surface molecular markers [27], flow cytometry analysis was conducted as explained before [28, 29]. Cells were incubated with monoclonal antibodies targeting specific surface markers such as *CD90*, *CD105*, *CD34*, and *CD45*, along with their respective matched-isotype controls. This rigorous methodology ensured accurate characterization and validation of MSC populations based on their surface marker expression profiles, thereby facilitating subsequent investigations into their role in AGA pathogenesis.

RNA extraction and quantitative analysis by real-time polymerase chain reaction (PCR)

First, total RNA was isolated from the cells with Favor-Prep Blood/Cultured Cell Total Mini Kit or (FAFB) mini column kit (Yekta Tajhiz Azma) according to the manufacturer's protocol. Second, 2 µl pure extracted RNA was used with dNTPs, Oligo(dt)18 primer, and 5X first-strand buffer to generate cDNA with PCR device. Then, the purity of cDNA was determined by Nano Drop Technique and gel electrophoresis. Third, quantitative reverse transcriptase PCR was carried out to determine the expression of genes encoding NAD-Dependent Protein Deacetylase Sirtuin-3 (*SIRT3*), NAD-Dependent Protein Deacetylase Sirtuin-7 (*SIRT7*), Nuclear Factor Of Activated T-Cells (*NFATC1*), Programmed Cell Death 1 Ligand 1 (*PDL-1*), and Glyceraldehyde-3-Phosphate Dehydrogenase (*GAPDH*) with Rotor-gene Q 6plex Platform device. Candidate gene primers, along with their product sizes and melting temperatures (Tm), are shown in Table 1. GAPDH values were used for normalizing. Gene expression was calculated using the ΔΔCt method [30].

Data processing method and software sources

Two sets of RNA-Seq raw data, (GSE212301) by Wu et al. [31] and (GSE101451) by Hu et al. [32], were downloaded from the Gene Expression Omnibus (https://www.ncbi.nlm.nih.gov/geo/) in HTTP format. The first dataset encompassed the whole transcriptome of HFs obtained from the vertex and occipital regions of several AGA-affected samples. Conversely, the second dataset comprised the whole transcriptome of bulge regions, which contain HFSCs, from the vertex and occipital regions of a subset of AGA-affected samples.

Statistical analyses, including the calculation and interpretation of Differentially Expressed Genes (DEGs), were conducted utilizing the R statistical software (version 4.4.0, https://www.r-project.org/). Subsequently, GO Enrichment analysis of the DEGs was performed using the WEB-based GEne SeT AnaLysis Toolkit (https://www.webgestalt.org/). This analysis encompassed biological process, cellular component, and molecular function categories based on Gene Set Enrichment Analysis (GSEA) as the enrichment method, along with the exploration of Kyoto Encyclopedia of Genes and Genomes (KEGG) pathways.

Table 1 candidate gene primers with their product size and temperature melt (TM)

Gene	Primer ID	Sequence	TM	Product size
NFATC1	*NFATC1-F*	CACCAAAGTCCTGGAGATCCCA	61.69	132 bp
	NFATC1-R	TTCTTCCTCCCGATGTCCGTCT	62.87	
SIRT7	*SIRT7-F*	TGGAGTGTGGACACTGCTTCAG	62.44	144 bp
	SIRT7-R	CCGTCACAGTTCTGAGACACCA	62.16	
SIRT3	*SIRT3-F*	CCCTGGAAACTACAAGCCCAAC	61.40	162 bp
	SIRT3-R	GCAGAGGCAAAGGTTCCATGAG	61.78	
PDL-1	*PDL-1-F*	TGCCGACTACAAGCGAATTACTG	61.22	150 bp
	PDL-1-R	CTGCTTGTCCAGATGACTTCGG	61.25	
GAPDH	*GAPDH-R*	GTCTCCTCTGACTTCAACAGCG	60.92	131 bp
	GAPDH-F	ACCACCCTGTTGCTGTAGCCAA	64.41	

Results

Determining the efficiency of primers and the purity of the PCR product by using gel electrophoresis

Following real-time PCR, gel electrophoresis was employed to assess the efficiency of primers and the purity of the PCR products. Notably, for each gene, bands of similar length to those anticipated based on BLAST analysis were observed (see Fig. 1). This consistency confirms the specificity of the amplification and the absence of non-specific products.

SIRT7 and *SIRT3* have lower gene expression in AGA-affected samples

To examine differential gene expression between AGA-affected samples (vertex regions) and control samples (occipital regions), comparative real-time PCR was utilized. The results, presented in Figs. 2-A and 3-A, highlight significant observations. Each pair of samples, consisting of an occipital (control) and a vertex

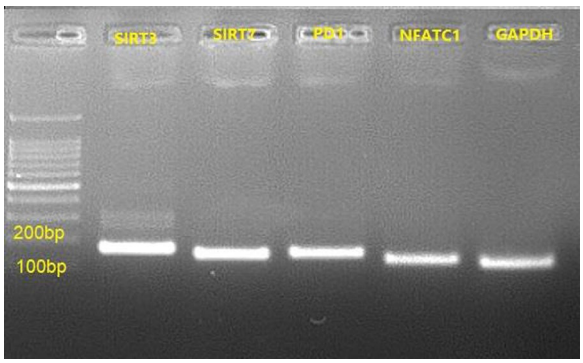

Fig. 1 cDNA bands on agarose gel electrophoresis. Each gene has a length between 100 to 200 bp

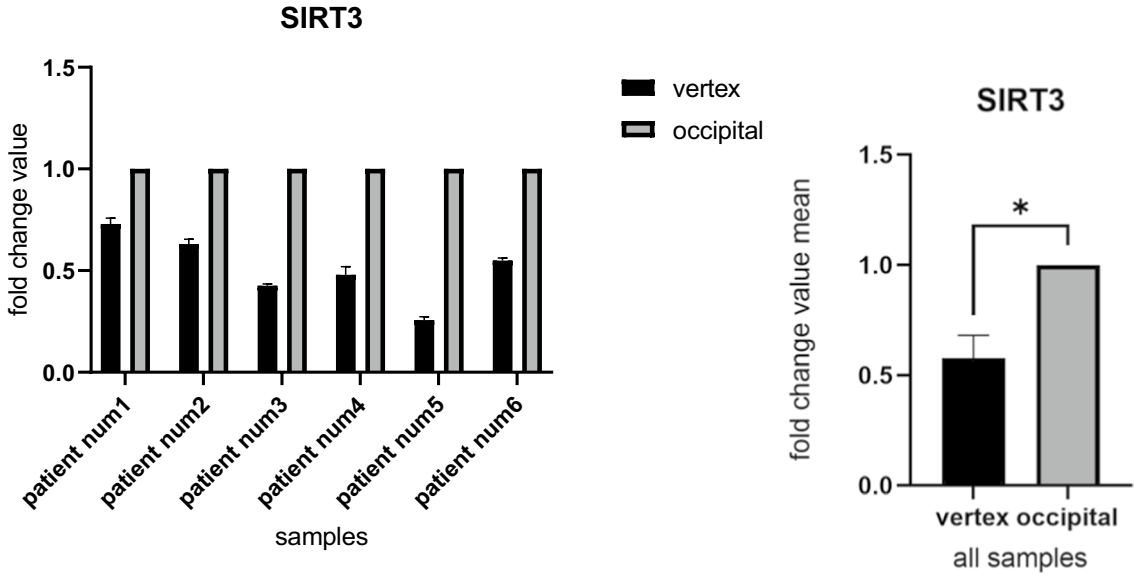

Fig. 2 **A**, **B** Different gene expression between control (occipital part) and AGA (vertex part) samples in each patient. In each graph, the horizontal axis represents the patient samples, while the vertical axis illustrates the fold change value. All AGA samples have lower expression (**A**). The average fold change ratio of *SIRT3* gene expression between the control and AGA-affected groups was statistically analyzed using a paired t-test ($p < 0.05$). The difference in gene expression was found to be statistically significant, with a p-value of 0.0431 (**B**)

(AGA-affected) tissue from the same patient, was analyzed and graphically depicted. This methodological approach was employed to ensure a detailed and comparative understanding of the gene expression patterns.

The mean expression levels across both sample sets demonstrated a statistically significant reduction in gene expression in the AGA-affected samples compared to controls, as illustrated in Figs. 2B and 3B. These differences were assessed using a paired t-test, yielding a p-value of < 0.05, indicating a meaningful reduction in gene expression levels in the AGA group.

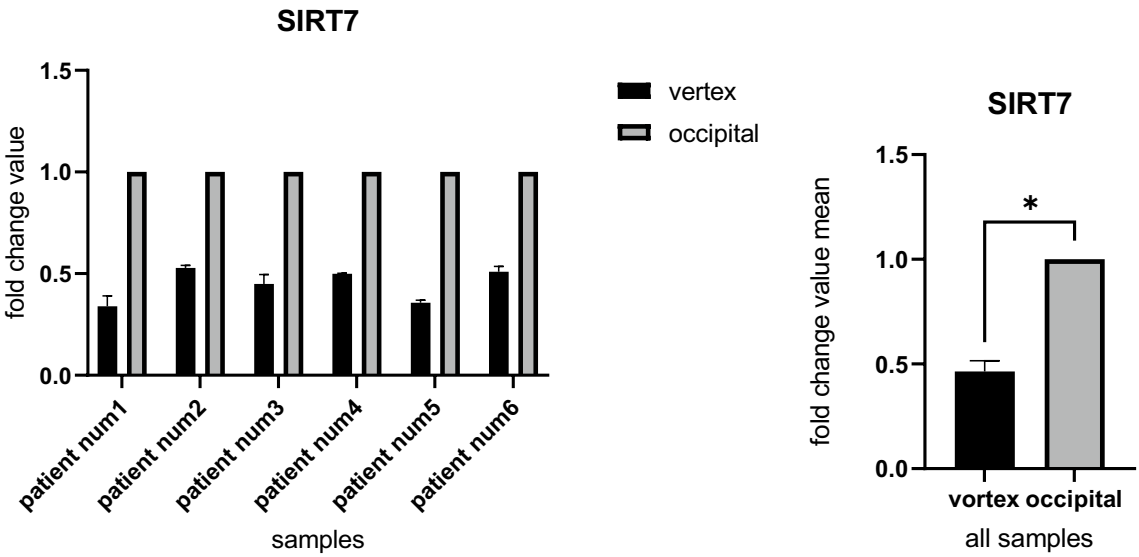

Fig. 3 **A**, **B** Different gene expression between control (occipital part) and AGA (vertex part) samples in each patient. In each graph, the horizontal axis represents the patient samples, while the vertical axis illustrates the fold change value. All AGA samples have lower expression (**A**). The average fold change ratio of *SIRT7* gene expression between the control and AGA-affected groups was statistically analyzed using a paired t-test ($p < 0.05$). The difference in gene expression was found to be statistically significant, with a p-value of 0.0301 (**B**)

NFATC1 and *PDL-1* have higher gene expression in AGA-affected samples

The results, as depicted in Figs. 4A and 5A, reveal important insights. Each pair of samples, consisting of occipital (control) and vertex (AGA-affected) tissues from the same patient, was analyzed and presented graphically. The data indicate consistently higher expression levels of *NFATC1* in the vertex regions compared to the occipital regions across all patient samples. However, the expression of the *PDL-1* gene presented mixed results; while some AGA-affected samples exhibited higher expression levels, in line with our initial

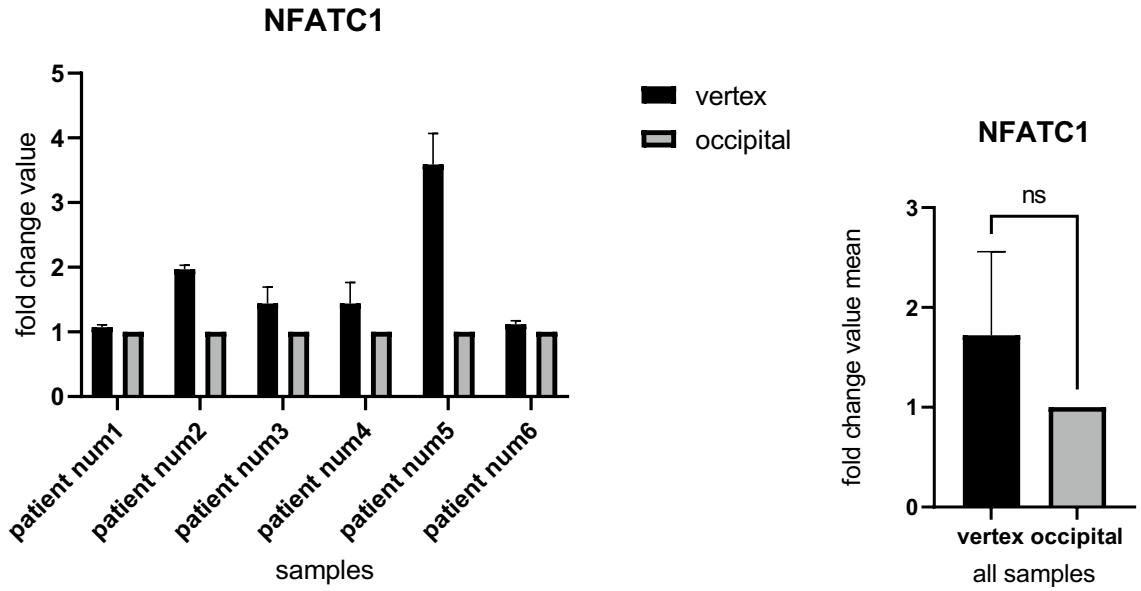

Fig. 4 **A**, **B** Different gene expression between control (occipital part) and AGA (vertex part) samples in each patient. In each graph, the horizontal axis represents the patient samples, while the vertical axis illustrates the fold change value (**A**). The average fold change ratio of *NFATC1* gene expression between the control and AGA-affected groups was statistically analyzed using a paired t-test ($p < 0.05$). The difference in gene expression was found to be statistically non-significant (**B**)

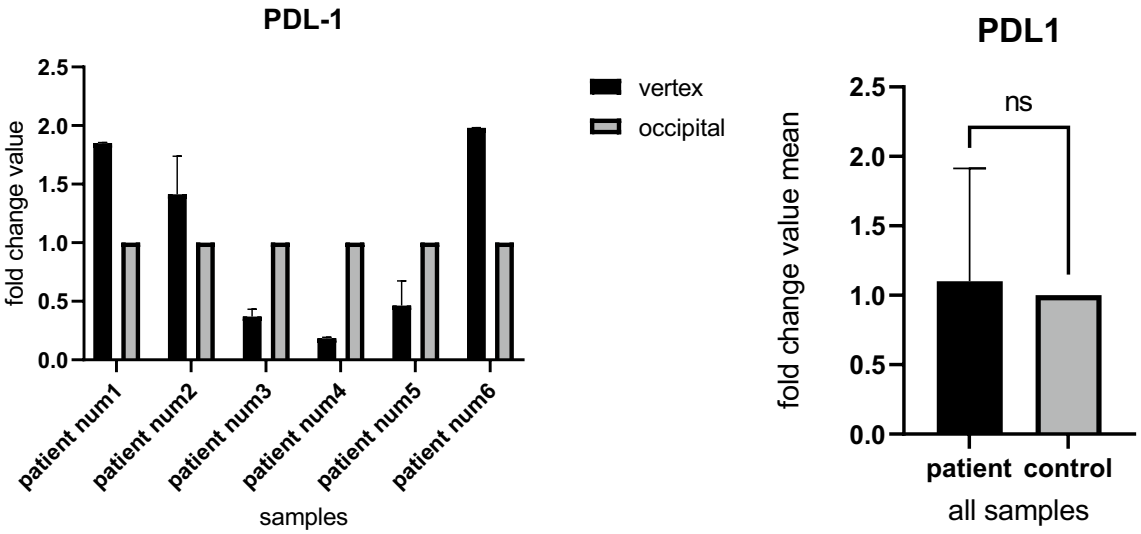

Fig. 5 **A**, **B** Different gene expression between control (occipital part) and AGA (vertex part) samples in each patient. In each graph, the horizontal axis represents the patient samples, while the vertical axis illustrates the fold change value. Results vary (**A**). The average fold change ratio of *PDL-1* gene expression between the control and AGA-affected groups was statistically analyzed using a paired t-test ($p < 0.05$). The difference in gene expression was found to be statistically non-significant (**B**)

hypothesis, others showed unexpectedly lower expression in the vertex regions.

The mean expression levels for both genes showed a statistically non-significant increase in the AGA-affected samples compared to the controls, as illustrated in Figs. 4B and 5B. A paired t-test was performed to evaluate these differences, and although the p-value was < 0.05, the observed variations in gene expression were not consistent enough to reach statistical significance for either gene.

Hierarchical clustering of differentially expressed genes (DEGs)

Hierarchical clustering was performed using the heatmap function from the ggplot2 library in R software to discern gene expression patterns between control samples and AGA-affected samples from first dataset (GSE212301). In the heatmap presented in Fig. 6, rows represent genes, while columns represent samples. Fifty differential genes, identified based on DESeq2 normalized gene expression with the lowest padj < 0.05, were included in the analysis.

The heatmap illustrates those genes with similar expression patterns are clustered together, with up-regulated genes depicted in red and down-regulated genes in blue. Notably, despite the inclusion of our gene of interest—*SIRT3*, *SIRT7*, *NFATC1*, and *PDL-1*- in the DEG Excel file which was calculated by using the first dataset (GSE212301), none of them were among the 50 genes exhibiting significant P values.

MA-plot and Volcano plot

In DESeq2, the plotMA function is employed to visualize the log2 fold change attributed to a given variable over the mean of normalized counts in an experiment with a two-group comparison within the DESeqDataSet. For our analysis, we utilized the first dataset (GSE212301) to generate Fig. 7 and the second dataset (GSE101451) to produce Fig. 8. Each plot represents individual genes as dots, with the x-axis denoting the average expression over all samples and the y-axis representing the log2 fold change between the normal and patient groups. These plots serve to illustrate that only genes with a large average normalized count contain sufficient information to yield a significant call. Genes exhibiting greater expression in AGA -affected samples are depicted in blue, whereas those with lower expression in AGA-affected samples are represented in red. The analysis depicted in Fig. 7 reveals a significant downregulation of *SIRT3* and *SIRT7* expression in AGA-affected samples compared to controls as *ATF3*, *PTGS2*, *SELENBP1*, *CA2*, *PTGS2* and *DAZ* genes have higher expression while *SIRT3*, *SIRT7*, *DGAT2L6* and *PTGDS* genes have lower expression in AGA-affected samples. Conversely, Fig. 8 illustrates a significant upregulation of *NFATC1* expression

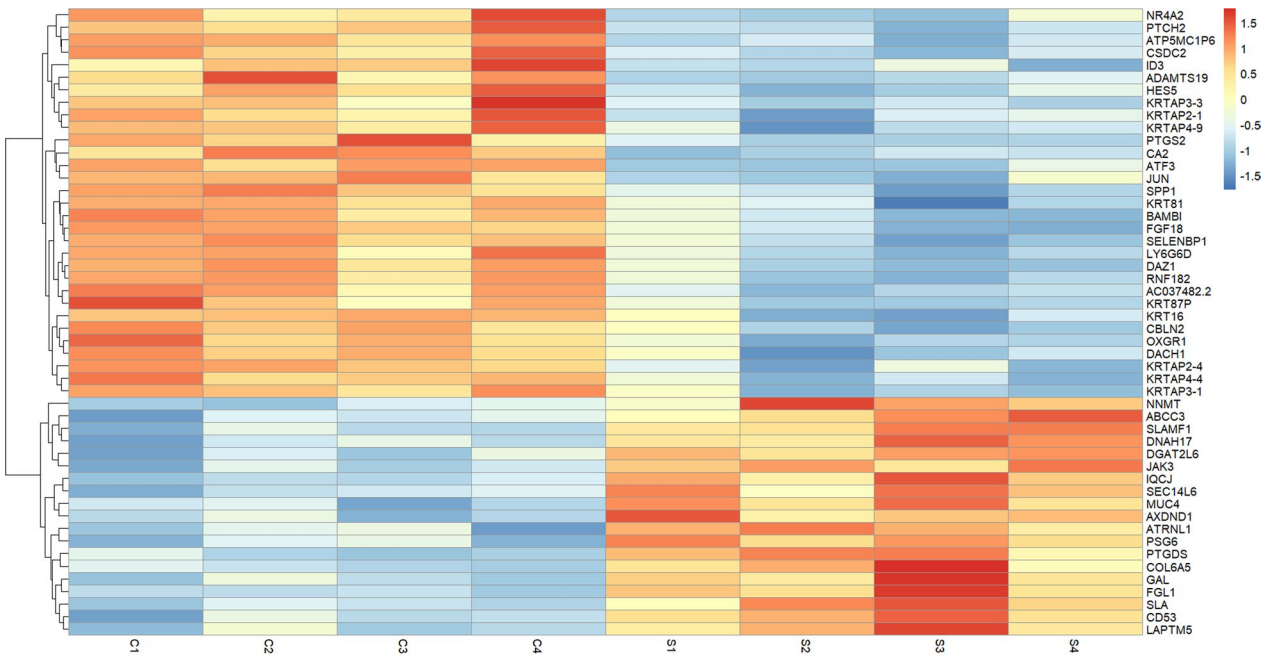

Fig. 6 Heatmap across all the samples using the top 50 most DE genes between the control and AGA patient groups, based on (GSE212301) dataset. rows represent genes, while columns represent samples. Fifty differential genes, identified based on DESeq2 normalized gene expression with the lowest padj < 0.05, were included in the analysis. genes with similar expression patterns are clustered together, with up-regulated genes depicted in red and down-regulated genes in blue

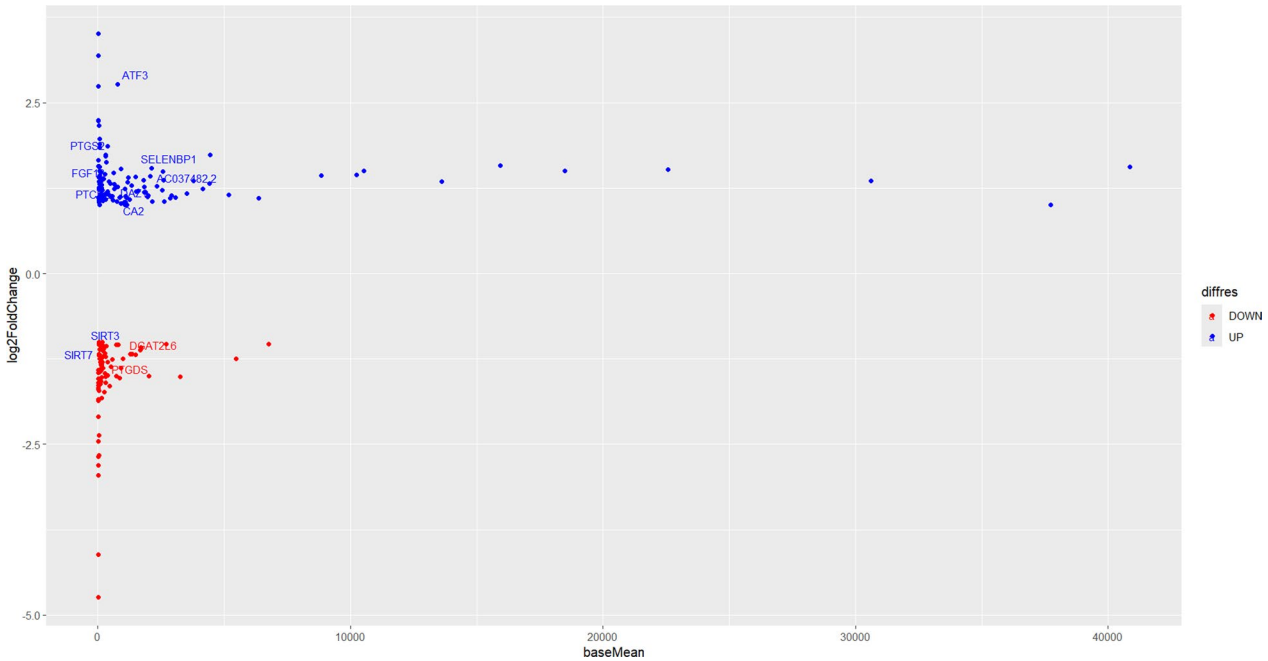

Fig. 7 MA plot from differential expression between control vs AGA patient groups, based on (GSE212301) dataset. plot represents individual genes as dots, with the x-axis denoting the average expression over all samples and the y-axis representing the log2 fold change between the normal and patient groups (padj < 0.05). Genes exhibiting greater expression in AGA-affected samples are depicted in blue, whereas those with lower expression in AGA-affected samples are represented in red

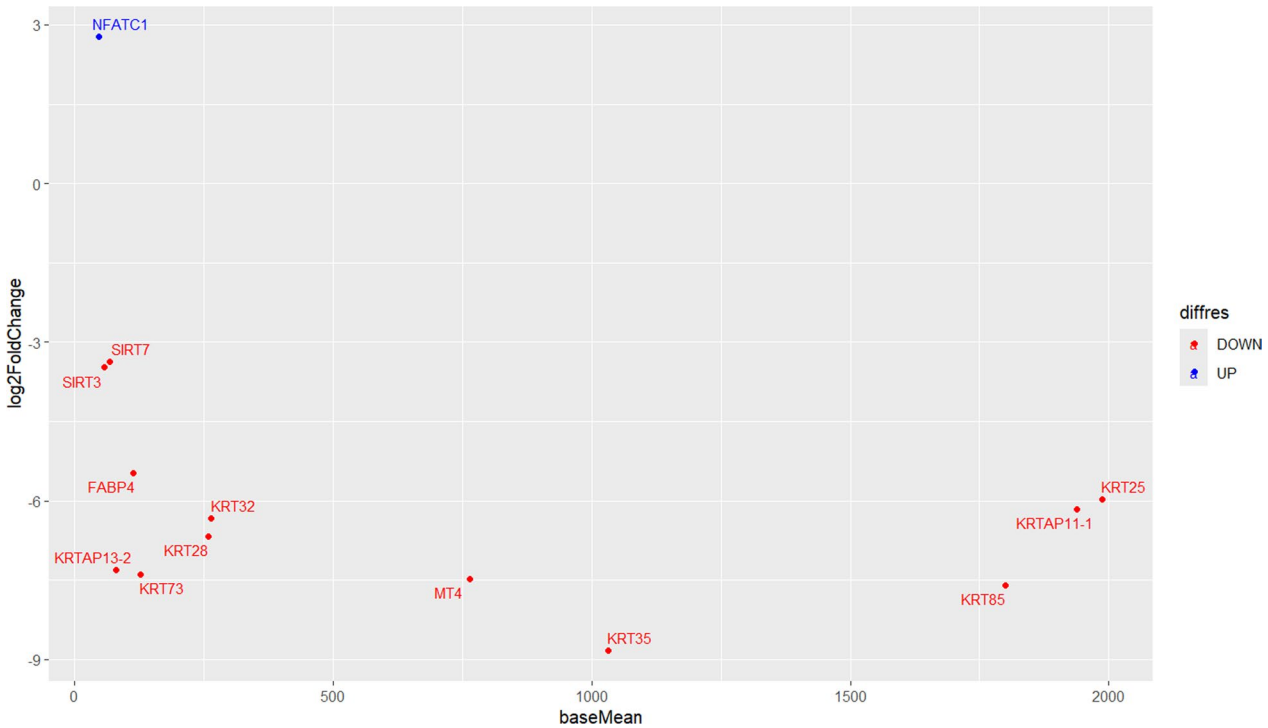

Fig. 8 MA plot from differential expression between control vs AGA patient groups, based on (GSE101451) dataset. plot represents individual genes as dots, with the x-axis denoting the average expression over all samples and the y-axis representing the log2 fold change between the normal and patient groups (padj < 0.05). Genes exhibiting greater expression in AGA-affected samples are depicted in blue, whereas those with lower expression in AGA-affected samples are represented in red

in AGA-affected samples. In Fig. 8, *NFATC1* gene has higher expression while *SIRT3*, *SIRT7*, *FABP4*, *KRT32*, *MT4*, *KRT28* and *KRT73* genes have lower expression in AGA-affected samples.

Figure 9 presents a volcano plot depicting differential gene expression based on the first dataset (GSE212301). The y-axis corresponds to the mean expression value of the negative logarithm (base 10) of the adjusted P-value, while the x-axis displays the log2 fold change (FC) value. In this plot, blue dots represent genes that are upregulated in expression (Padj < 0.05, log2 FC > 1) between control and AGA-affected samples, while red dots represent genes that are downregulated in expression (Padj < 0.05, log2 FC < − 1) between these groups. As indicated by the plot, *SIRT3* and *SIRT7* exhibit lower expression levels in AGA-affected samples compared to controls.

Functional analysis of DEGs

To identify functional categories of differentially expressed genes, Gene Ontology (GO) enrichment analysis was performed using the WEB-based GEne SeT AnaLysis Toolkit (https://www.webgestalt.org/). The groups with an Padj < 0.05 were examined. Gene ontology (GO) was applied to identify characteristic biological attributes of the first RNA-seq dataset (GSE212301). Results were classified into different functional categories for biological process, molecular process, and cellular component (Fig. 10).

Kyoto Encyclopedia of Genes and Genomes (KEGG) pathway analysis

To explore the activation and suppression of Differentially Expressed Genes (DEGs) within different classes of pathways, gene expression data was mapped to the Kyoto Encyclopedia of Genes and Genomes (KEGG) pathway using the WEB-based GEne SeT AnaLysis Toolkit (https://www.webgestalt.org/). This analysis was based on the first RNA-seq dataset (GSE212301), and illustrates the top ten enriched pathways identified through this analysis (Fig. 11).

Discussion

The aging process exerts its effects on HFs through two distinct mechanisms: external aging mechanisms and internal aging mechanisms. External aging mechanisms encompass alterations within the niche environment, characterized by physical atrophy and perturbations in the secretion of crucial factors [33]. Conversely, internal aging mechanisms involve alterations in functional pathways intrinsic to hair HF physiology, notably including the Wnt/β-catenin and BMP pathways [34].

The Wnt pathway plays a pivotal role in instigating the onset of a new hair cycle within HFSCs [35]. However,

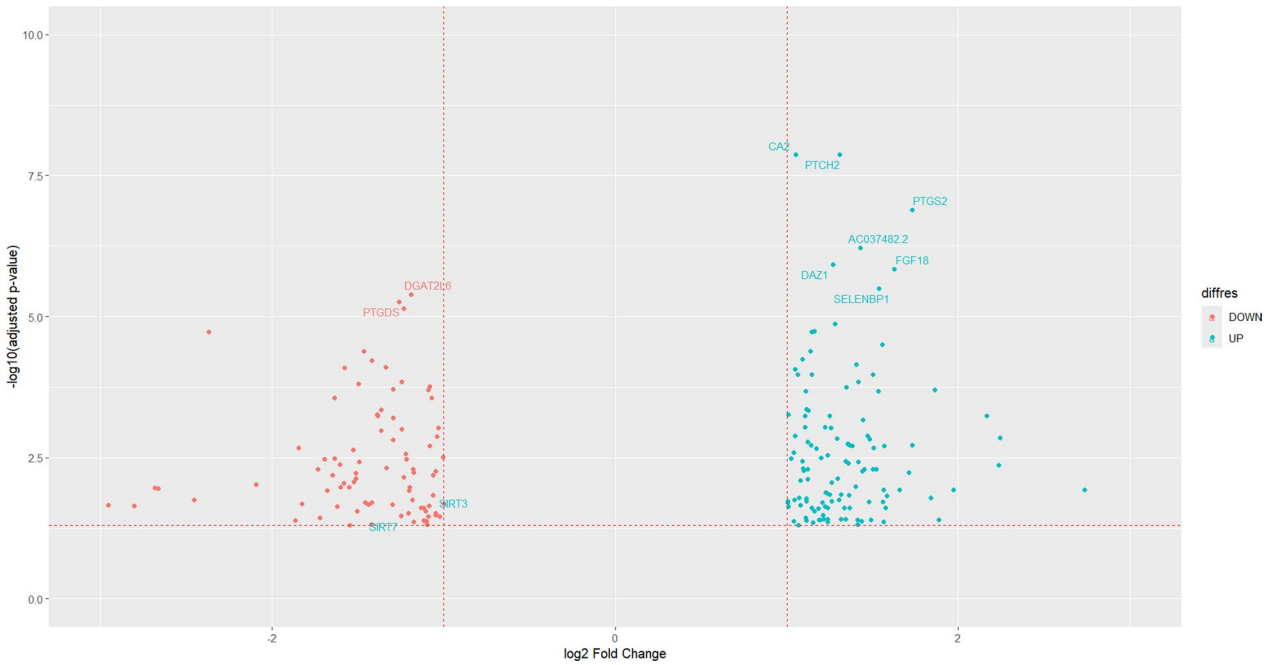

Fig. 9 Volcano plot of the differentially expressed genes between control and AGA patient groups. Red vertical lines highlight log fold changes of -1 and 1, while red horizontal lines represent a Padj of 0.05, based on (GSE212301) dataset. In this plot, blue dots represent genes that are upregulated in expression (Padj < 0.05, log2 FC > 1) between control and Androgenetic Alopecia (AGA) patient groups, while red dots represent genes that are downregulated in expression (Padj < 0.05, log2 FC < − 1) between these groups

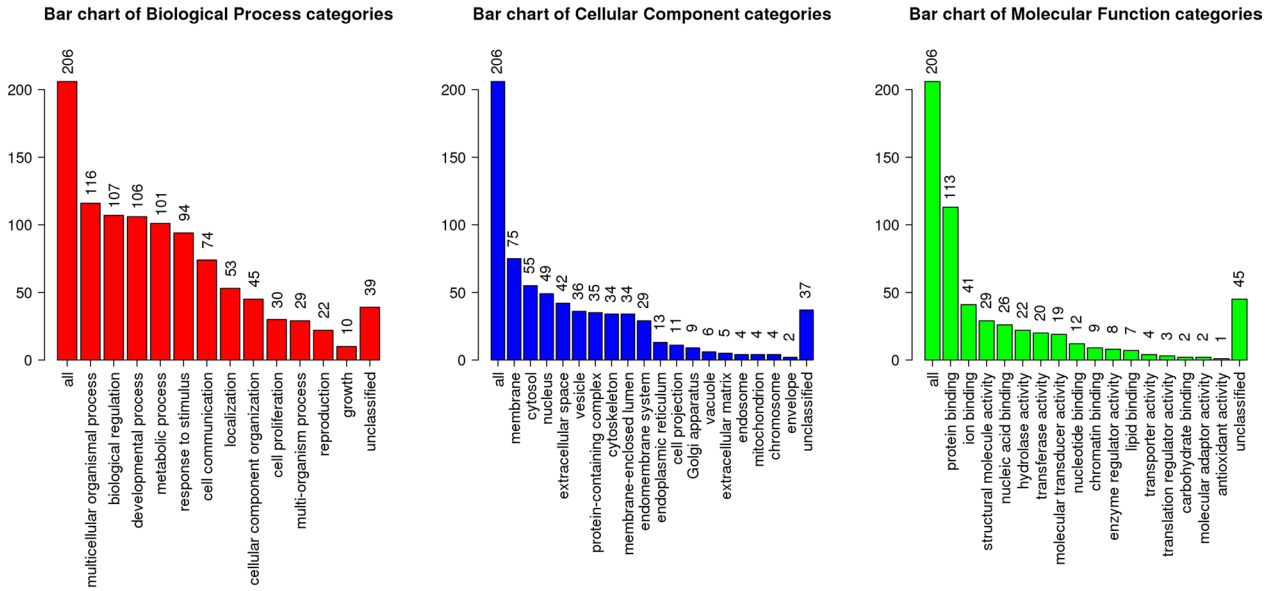

Fig. 10 Gene Ontology analysis of biological process,cellular component, and molecular function for the genes which have the most significant Pvalues, based on the first RNA-seq (GSE212301) dataset

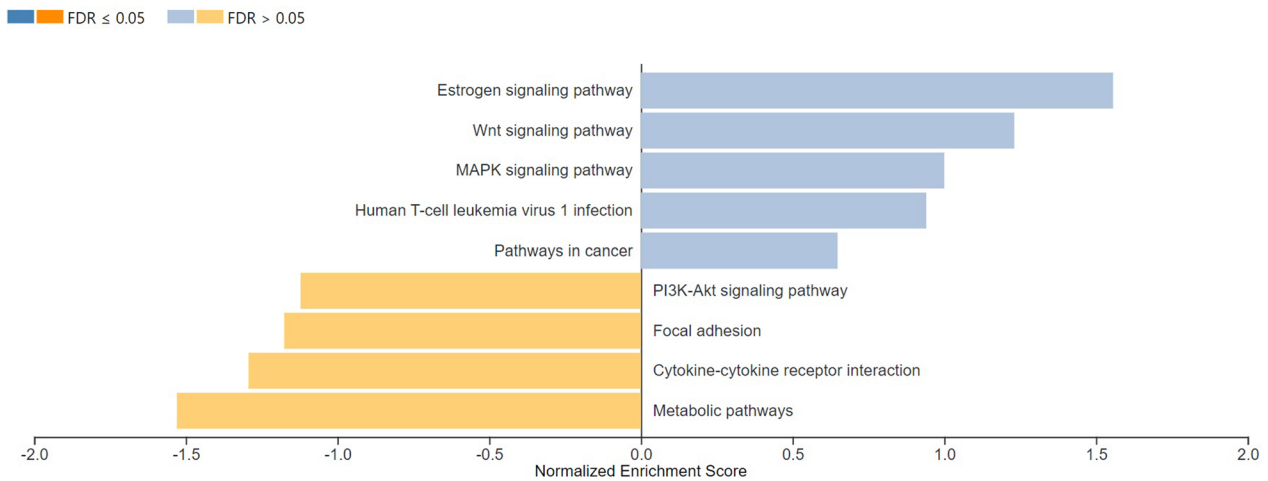

Fig. 11 Kyoto Encyclopedia of genes and genomes (KEGG) pathway enrichment for up- and down-regulated genes between control and AGA patient groups. Up-regulated groups are shown in blue, while the down-regulated groups are shown in orange, based on the first RNA-seq (GSE212301) dataset

during the Telogen phase or as a consequence of aging, this pathway has some interaction [36] with the BMP pathway. The BMP pathway is responsible for maintaining cells in a state of rest or quiescence, primarily through the upregulation of the *NFATC1* gene expression [15].

In this study, we indicated *NFATC1* gene expression is more in AGA-affected samples, but the mean expression level showed a statistically non-significant increase in the AGA-affected samples compared to the controls. However, RNA-Seq analysis proved our results by a meaningful P-value. In addition, the graph in Fig. 11 depicting the higher function of the Wnt signaling pathway in AGA-affected samples aligns with our experimental and bioinformatic findings, which revealed higher expression levels of *NFATC1* in AGA-affected samples. Indeed, the Wnt pathway is pivotal in regulating hair follicle cycling and is implicated in various aspects of hair biology, including hair loss and graying during aging.

sirt7 gene in HFSCs of aged mice has lower expression compared to their youthful counterparts [17]. Notably,

SIRT7 encodes a nuclear deacetylase, functioning as an upregulator for *NFATC1* gene expression [18]. Thus, one possible explanation for the observed increase in *NFATC1* gene expression in aged HFSCs may be attributed to the decreased expression of the *SIRT7* gene [17]. This elucidates a potential molecular mechanism underlying the dysregulation of *NFATC1* gene expression in the context of aging-related changes in HFSCs, and our finding has showed the same results.

According to our functional bioinformatic analysis, The observed decrease in metabolic pathway activation, coupled with the downregulation of *SIRT3* and *SIRT7*, which are members of the metabolic pathway, underscores the intricate interplay between metabolic dysregulation and HF biology in the pathogenesis of AGA.

Mitochondrial damages in dermal papilla cells of HFs who were affected by AGA have higher level, compared to those of healthy HFs [37]. This pronounced mitochondrial damage was also observed in aged HFs when juxtaposed with their youthful counterparts [38]. Considering that one of the pivotal regulators of mitochondrial function is *SIRT3*, a mitochondrial deacetylase [20], we proposed the hypothesis that dysregulation of *SIRT3* gene expression may play a role in the pathogenesis of AGA.

By blocking the *PD-1/PDL-1* pathway, hair growth has observed to improve in cancer patients [39]. In addition, the *pd-1/pdl-1* signaling pathway may act as an inhibitor of hair growth in mice [20]. Given that the activity of this signaling pathway intensifies with advancing age, coupled with evidence suggesting a correlation between increased expression of *NFATC1* and *PDL-1* genes during aging [40, 41], we hypothesize that the heightened expression of the *PDL-1* gene due to aging may exert effects on AGA. However, our findings did not prove our hypothesis, moreover, our subsequent RNA-Seq analysis showed that the corresponding P-value did not meet the significance threshold.

Based on the results that are showed in Fig. 10, it appears that Cell proliferation and reproduction are key biological processes implicated in the pathophysiology of AGA. While these processes are broad and not exclusive to AGA, their dysregulation may contribute to impaired HF function. Specifically, disruptions in these processes can inhibit the proliferation of hair follicle stem cells and interfere with the activation of the hair growth cycle, ultimately leading to the hair loss characteristic of AGA.

Furthermore, this functional study revealed that genes exhibiting the most significant differences between control and AGA-affected samples predominantly belong to the membrane category within the cellular component classification. As PDL-1 protein is one of the cell adhesion molecules (according to KEGG analysis), different expression level of this gene in AGA group was predicted.

Overall, The multifaceted role of *PDL-1* in diverse signaling pathways suggests that its expression levels may vary widely across different health conditions and among individuals. These variations may contribute to the complex pathophysiology of AGA and underscore the need for comprehensive analysis approaches that account for such intricacies.

Limitations

Due to budgetary constraints and other conditions, only a small number of samples were tested. Future studies with a larger cohort are recommended to draw more robust conclusions. Additionally, to gain a deeper understanding of the role and effect of the PDL-1 gene, further research should consider all factors influencing its expression across different signaling pathways. The variability in PDL-1 expression across pathways necessitates comprehensive evaluation to ensure reliable results.

Conclusion

Our results reveal that *SIRT3* and *SIRT7* exhibit statistically significant differences in gene expression levels between control (occipital part) and AGA-affected (vertex part) groups. This observation highlights the importance of these genes in AGA pathology.

However, while *NFATC1* and *PDL-1* also showed different expression levels between control samples and AGA-affected samples, no definitive conclusions could be drawn due to the fact that their gene expression level differences were not statistically significant. Similarly, our RNA-Seq analysis suggests that the differential expression of *PDL-1* may not be significant. These discrepancies underscore the complexity of AGA pathogenesis and emphasize the importance of integrating experimental and computational approaches to gain a comprehensive understanding of the molecular mechanisms underlying this condition.

Overall, our findings suggest that while *SIRT3* and *SIRT7* may play critical roles in AGA development, further research is needed to elucidate the significance of *NFATC1* and *PDL-1* in this context and to explore their potential as therapeutic targets for AGA treatment.

Abbreviations

AGA	Androgenetic alopecia
HF	Hair follicle
HFSC	Hair follicle stem cell
MSC	Mesenchymal stem cell

Acknowledgements

This study was technically supported by Dena and Sava Genome genetic laboratories.

Author contributions

Hadis Abbasian: the experimental part of the research, manuscript writing, and bioinformatic analysis were conducted by Hadis Abbasian. Dr. Mehrdad Noruzinia: the initial idea and planning for the methodology and

data processing were provided by Dr. Mehrdad Noruzinia. Dr. Dr Masoud Garshasbi: the corresponding author, oversaw and verified all processes. Additionally, his laboratory provided technical assistance during the experimental phase of the research.

Funding
This research received no specific grant from any funding agency in the public, commercial, or not-for-profit sectors.

Data availability
The RNA-Seq datasets analyzed in this study, GSE212301 by Wu W, Tang Y, et al., and GSE101451 by Hu Z, Qu Q, et al., are publicly available from the Gene Expression Omnibus (GEO) repository at https://www.ncbi.nlm.nih.gov/geo/.

Declarations

Ethical approval and consent to participate
This research was approved by the Ethics Committee of Tarbiat Modares University (IR.MODARES.REC.1402.244), Tehran, Iran. All the participants have accepted and signed the informed consent during the standard genetic counselling sessions. Written informed consent was obtained from the patients for publication of this study. A copy of the written consent is available for review by the Editor of this journal.

Consent for publication
All authors reviewed the results and approved the final version of the manuscript.

Competing interests
The authors declare no competing interests.

Received: 10 June 2024 Accepted: 15 October 2024
Published online: 21 November 2024

References

1. Heilmann S, Brockschmidt FF, Hillmer AM, Hanneken S, Eigelshoven S, Ludwig KU, et al. Evidence for a polygenic contribution to androgenetic alopecia. Br J Dermatol. 2013;169(4):927–30.
2. Ellis JA, Sinclair R, Harrap SB. Androgenetic alopecia: pathogenesis and potential for therapy. Expert Rev Mol Med. 2002;4(22):1–11.
3. Hamilton JB. Patterned loss of hair in man: types and incidence. Ann N Y Acad Sci. 1951;53(3):708–28. https://doi.org/10.1111/j.1749-6632.1951.tb31971.x.
4. Sinclair R. Male pattern androgenetic alopecia. BMJ. 1998;317(7162):865–9.
5. Kidangazhiathmana A, Santhosh P. Pathogenesis of androgenetic alopecia. Clin Dermatol Rev. 2022;6(2):69–74.
6. Higgins CA, Westgate GE, Jahoda CA. From telogen to exogen: mechanisms underlying formation and subsequent loss of the hair club fiber. J Invest Dermatol. 2009;129(9):2100–8.
7. Jahoda CAB. Cellular and developmental aspects of androgenetic alopecia. Exp Dermatol. 1998;7(5):235–48. https://doi.org/10.1111/j.1600-0625.2007.00666.x.
8. Harrison S, Sinclair R. Telogen effluvium. Clin Exp Dermatol. 2002;27(5):389–95.
9. Mistriotis P, Andreadis ST. Hair follicle: a novel source of multipotent stem cells for tissue engineering and regenerative medicine. Tissue Eng Part B Rev. 2013;19(4):265–78. https://doi.org/10.1089/ten.teb.2012.0422.
10. Rabbani P, Takeo M, Chou W, Myung P, Bosenberg M, Chin L, et al. Coordinated activation of Wnt in epithelial and melanocyte stem cells initiates pigmented hair regeneration. Cell. 2011;145(6):941–55.
11. Ahmadvand M, Noruzinia M, Fard AD, Zohour MM, Tabatabaiefar MA, Soleimani M, et al. The role of epigenetics in the induction of fetal hemoglobin: a combination therapy approach. Int J Hematol-Oncol Stem Cell Res. 2014;8(1):9.
12. Taghizadeh M, Noruzinia M. Lovastatin reduces stemness via epigenetic reprograming of BMP2 and GATA2 in human endometrium and endometriosis. Cell J. 2017;19(1):50.
13. Rushton H, James KC, Mortimer CH. The unit area trichogram in the assessment of androgen-dependent alopecia. Br J Dermatol. 1983;109(4):429–37.
14. Tanimura S, Tadokoro Y, Inomata K, Binh NT, Nishie W, Yamazaki S, et al. Hair follicle stem cells provide a functional niche for melanocyte stem cells. Cell Stem Cell. 2011;8(2):177–87.
15. Hsu YC, Pasolli HA, Fuchs E. Dynamics between stem cells, niche, and progeny in the hair follicle. Cell. 2011;144(1):92–105.
16. Horsley V, Aliprantis AO, Polak L, Glimcher LH, Fuchs E. NFATc1 balances quiescence and proliferation of skin stem cells. Cell. 2008;132(2):299–310.
17. Li G, Tang X, Zhang S, Jin M, Wang M, Deng Z, et al. SIRT 7 activates quiescent hair follicle stem cells to ensure hair growth in mice. EMBO J. 2020;39(18): e104365. https://doi.org/10.15252/embj.2019104365.
18. Bosch-Presegue L, Vaquero A. Sirtuins in stress response: guardians of the genome. Oncogene. 2014;33(29):3764–75.
19. Mu WC, Ohkubo R, Widjaja A, Chen D. The mitochondrial metabolic checkpoint in stem cell aging and rejuvenation. Mech Age Dev. 2020;188:111254.
20. Zhou L, Wen L, Sheng Y, Lu J, Hu R, Wang X, et al. The PD-1/PD-L1 pathway in murine hair cycle transition: a potential anagen phase regulator. Arch Dermatol Res. 2021;313(9):751–8. https://doi.org/10.1007/s00403-020-02169-9.
21. Love MI, Huber W, Anders S. Moderated estimation of fold change and dispersion for RNA-seq data with DESeq2. Genome Biol. 2014;15(12):550. https://doi.org/10.1186/s13059-014-0550-8.
22. Huber W, Carey VJ, Gentleman R, Anders S, Carlson M, Carvalho BS, et al. Orchestrating high-throughput genomic analysis with bioconductor. Nat Methods. 2015;12(2):115–21.
23. Anders S, Huber W. Differential expression analysis for sequence count data. In: Nature Precedings. 2010. pp. 1–1. https://www.nature.com/articles/npre.2010.4282.1. Accessed 9 May 2024.
24. Li J, Tibshirani R. Finding consistent patterns: a nonparametric approach for identifying differential expression in RNA-Seq data. Stat Methods Med Res. 2013;22(5):519–36. https://doi.org/10.1177/0962280211428386.
25. Ashburner M, Ball CA, Blake JA, Botstein D, Butler H, Cherry JM, et al. Gene ontology: tool for the unification of biology. Nat Genet. 2000;25(1):25–9.
26. Kanehisa M, Goto S. KEGG: Kyoto encyclopedia of genes and genomes. Nucl Acids Res. 2000;28(1):27–30.
27. Dominici M, Le Blanc K, Mueller I, Slaper-Cortenbach I, Marini FC, Krause DS, et al. Minimal criteria for defining multipotent mesenchymal stromal cells: The International Society for Cellular Therapy position statement. Cytotherapy. 2006;8(4):315–7.
28. Farshdousti Hagh M, Noruzinia M, Mortazavi Y, Soleimani M, Kaviani S, Mahmodinia Maymand M. Zoledrinic acid induces steoblastic differentiation of mesenchymal stem cells without change in hypomethylation status of OSTERIX promoter. Cell J. 2012;14(2):90–7.
29. Hagh MF, Noruzinia M, Mortazavi Y, Soleimani M, Kaviani S, Abroun S, et al. Different methylation patterns of RUNX2, OSX, DLX5 and BSP in osteoblastic differentiation of mesenchymal stem cells. Cell J. 2015;17(1):71.
30. Livak KJ, Schmittgen TD. Analysis of relative gene expression data using real-time quantitative PCR and the 2- ΔΔCT method. Methods. 2001;25(4):402–8.
31. GEO Accession viewer [A novel Long non-coding RNA AL136131.3 inhibits hair growth through mediating glycolysis in androgen alopecia]. https://www.ncbi.nlm.nih.gov/geo/query/acc.cgi?acc=GSE212301. Accessed 9 May 2024.
32. GEO Accession viewer [Transcripotome analysis of different locations of hair follicles (bulb, bulge) in androgenetic alopecia]. https://www.ncbi.nlm.nih.gov/geo/query/acc.cgi?acc=GSE101451. Accessed 9 May 2024.
33. Jang H, Jo Y, Lee JH, Choi S. Aging of hair follicle stem cells and their niches. BMB Rep. 2023;56(1):2.
34. Keyes BE, Segal JP, Heller E, Lien WH, Chang CY, Guo X, et al. Nfatc1 orchestrates aging in hair follicle stem cells. Proc Natl Acad Sci USA. 2013. https://doi.org/10.1073/pnas.1320301110.
35. Botchkarev VA, Botchkareva NV, Nakamura M, Huber O, Funa K, Lauster R, et al. Noggin is required for induction of the hair follicle growth phase in postnatal skin. FASEB J. 2001;15(12):2205–14. https://doi.org/10.1096/fj.01-0207com.

36. Kobielak K, Stokes N, De La Cruz J, Polak L, Fuchs E. Loss of a quiescent niche but not follicle stem cells in the absence of bone morphogenetic protein signaling. Proc Natl Acad Sci USA. 2007;104(24):10063–8. https://doi.org/10.1073/pnas.0703004104.
37. Bahta AW, Farjo N, Farjo B, Philpott MP. Premature senescence of balding dermal papilla cells in vitro is associated with p16INK4a expression. J Invest Dermatol. 2008;128(5):1088–94.
38. Singh B, Schoeb TR, Bajpai P, Slominski A, Singh KK. Reversing wrinkled skin and hair loss in mice by restoring mitochondrial function. Cell Death Dis. 2018;9(7):735.
39. Rivera N, Boada A, Bielsa MI, Fernández-Figueras MT, Carcereny E, Moran MT, et al. Hair repigmentation during immunotherapy treatment with an anti–programmed cell death 1 and anti–programmed cell death ligand 1 agent for lung cancer. JAMA Dermatol. 2017;153(11):1162–5.
40. Kugel CH III, Douglass SM, Webster MR, Kaur A, Liu Q, Yin X, et al. Age correlates with response to anti-PD1, reflecting age-related differences in intratumoral effector and regulatory T-cell populations. Clin Cancer Res. 2018;24:5347.
41. Pippin JW, Kaverina N, Wang Y, Eng DG, Zeng Y, Tran U, et al. Upregulated PD-1 signaling antagonizes glomerular health in aged kidneys and disease. J Clinl Invest. 2022;132(16): e156250.

Publisher's Note